Supplementary Information for

Understanding Climate Change Impacts on Drought in China over the 21st century: A Multi-Model Assessment from CMIP6

Feng Xu[1#], Yanping Qu [2#], Virgílio A. Bento[3], Hongquan Song[4], Jianxiu Qiu[5], Junyu Qi[6], Lingling Wan[1], Rongrong Zhang[1], Miao Lijuan[7], Xuesong Zhang[8], Qianfeng Wang[1, 9*]

[1]*Fujian Provincial Key Laboratory of Remote Sensing of Soil Erosion and Disaster Protection/College of Environmental & Safety Engineering, Fuzhou University, Fuzhou, 350116, China*

[2]*Research Center on Flood and Drought Disaster Reduction, China Institute of Water Resources and Hydropower Research, Beijing, 100038, China*

[3]*Instituto Dom Luiz, Faculdade de Ciências, Universidade de Lisboa, 1749-016 Lisboa, Portugal*

[4]*Institute of Urban Big Data, College of Geography and Environmental Science, Henan University, Kaifeng 475004, China.*

[5]*Guangdong Provincial Key Laboratory of Urbanization and Geo-simulation, School of Geography and Planning, Sun Yat-sen University, Guangzhou, 510275, China*

[6]*Earth System Science Interdisciplinary Center, University of Maryland, College Park, 5825 University Research Ct, College Park, MD 20740, USA*

[7]*School of Geographical Sciences, Nanjing University of Information Science and Technology, Nanjing 210044, China*

[8]*USDA-ARS Hydrology and Remote Sensing Laboratory Bldg. 007, Rm. 104, BARC-West Beltsville, MD 20705-2350, USA*

[9]*Key Lab of Spatial Data Mining & Information Sharing, Ministry of Education of China, Fuzhou, 350116, China*

*Corresponding author: Qianfeng Wang. E-mail: wangqianfeng@fzu.edu.cn

[#]These authors contribute equally. Feng Xu and Yanping Qu are the first authors.

Contents of this file

Supplementary Method 1. Calculation method of net radiation

The net surface radiation (R_n) is obtained by summing up the net surface shortwave (R_{ns}) and longwave (R_{nl}) radiation [1]:

$$R_{\mathrm{n}} = R_{ns} + R_{nl} = \left(\overline{R}_{s\downarrow} - \overline{R}_{s\uparrow}\right) + \left(\overline{R}_{l\downarrow} - \overline{R}_{l\uparrow}\right) \quad (1)$$

Where $\overline{R}_{s\downarrow}$ is downward shortwave radiation, $\overline{R}_{s\uparrow}$ is upward shortwave radiation, $\overline{R}_{l\downarrow}$ is downward longwave radiation, $\overline{R}_{l\uparrow}$ is upward longwave radiation. The upper horizontal line indicates that the data are bias-adjusted.

In ISIMIP3b, only the bias-adjusted $\overline{R}_{s\downarrow}$ and $\overline{R}_{l\downarrow}$ data are provided. The limitation of historical measured data makes it difficult to correct $\overline{R}_{s\uparrow}$ and $\overline{R}_{l\uparrow}$ with measured data. So we obtain $R_{s\uparrow}$ and $R_{l\uparrow}$ data from CMIP6, and then combine the empirical equations and the bias-adjusted $\overline{R}_{s\downarrow}$ and $\overline{R}_{l\downarrow}$ data to estimate the $\overline{R}_{s\uparrow}$ and $\overline{R}_{l\uparrow}$ data.

The shortwave albedo (α) is calculated as [1]:

$$\alpha = \frac{R_{s\uparrow}}{R_{s\downarrow}} \quad (2)$$

So the bias-adjusted $\overline{R}_{s\uparrow}$ is calculated as:

$$\overline{R}_{s\uparrow} = \alpha \overline{R}_{s\downarrow} \quad (3)$$

For downward longwave radiation ($R_{l\downarrow}$), the parameterized method suggested by Brutsaert (1975), which uses measurements of meteorological variables near the surface has been employed:

$$R_{l\downarrow} = \varepsilon_{\alpha} \sigma T_{\alpha}^{4} \quad (4)$$

where ε_{α} is atmospheric emissivity, T_{α} is air temperature in ˚C, σ = Stefan-Boltzmann constant.

The upward longwave radiation ($R_{l\uparrow}$) is calculated from the Stefan-Boltzmann

equation using land surface temperature:

$$R_{l\uparrow} = \varepsilon \sigma T_s^4 \quad (5)$$

where ε is land surface emissivity, T is land surface temperature in K.

Combining equations (4) and (5) with the available data, the bias-adjusted $\overline{R}_{l\uparrow}$ is calculated as,

$$\overline{R}_{l\uparrow} = \frac{R_{l\uparrow}}{R_{l\downarrow}} \frac{T_a^4}{\overline{T}_a^4} \overline{R}_{l\downarrow} \quad (6)$$

where T_a^4 is air temperature in ˚C, $\overline{T}_a^4$ is the bias-adjusted air temperature in ˚C.

Supplementary Method 2. Calculation equation of PM-RC model

$$E_p = \frac{0.408 s R_n + \gamma \frac{900}{T+273} uV}{\mathrm{s} + \gamma \left(1 + 0.34u\right)} \quad (7)$$

Where E_p is the atmospheric evaporative demand on the idealized grass surface (mm d^{-1}), s is the slope of the saturation vapor pressure curve (kPa ℃$^{-1}$) at the near-surface air temperature T (℃), R_n is the surface net radiation (MJ m^{-2} d^{-1}), γ is the psychrometric constant (kPa ℃$^{-1}$), u is the 2 m wind speed (m s^{-1}), and V is the difference between the saturation and the actual vapor pressure (kPa).

Supplementary Method 3. Calculation equation of PM-CO_2 model

$$E_p = \frac{0.408 s R_n + \gamma \frac{900}{T+273} uV}{\mathrm{s} + \gamma \left\{1 + u[0.34 + 2.4 \times 10^{-4} \left([CO_2] - 300\right)]\right\}} \quad (8)$$

Where [CO_2] denotes the atmospheric CO_2 concentration (ppm).

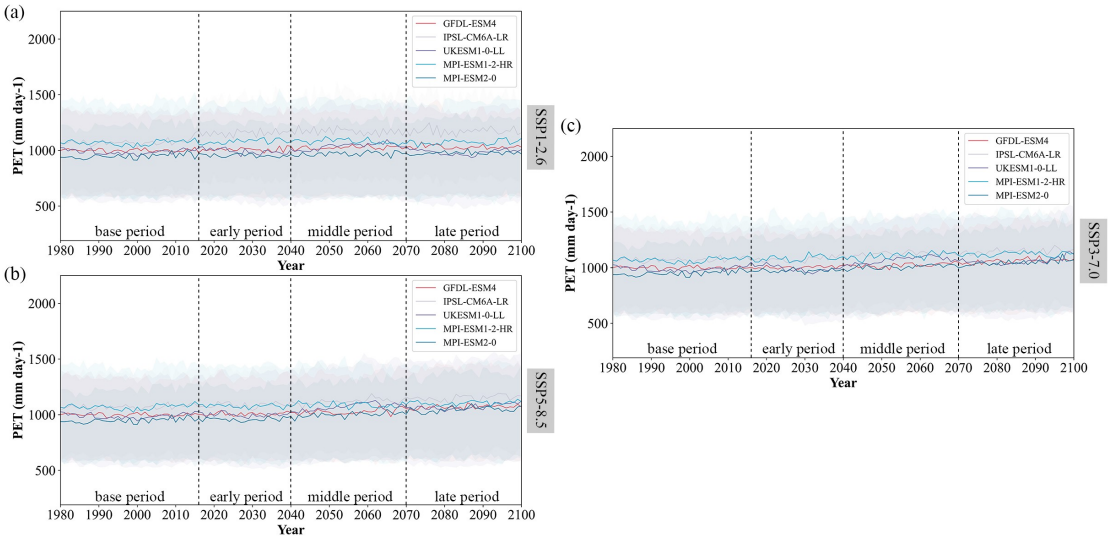

Supplementary Figure 1. Time series of PET calculated from PM-RC under (a) SSP1-2.6, (c) SSP3-7.0 and (b) SSP5-8.5 by five GCMs. Note: the solid line represents the annual mean of all global grids, while the shades represent the lower (25th percentile) and upper limits (75th percentile).

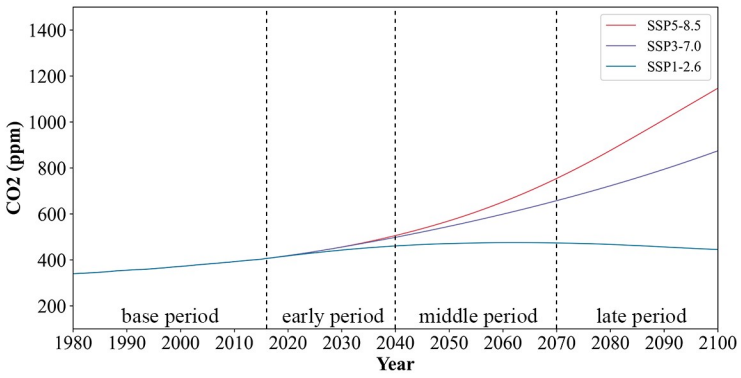

Supplementary Figure 2. Time series of CO_2 concentration under SSP1-2.6, SSP3-7.0 and SSP5-8.5.

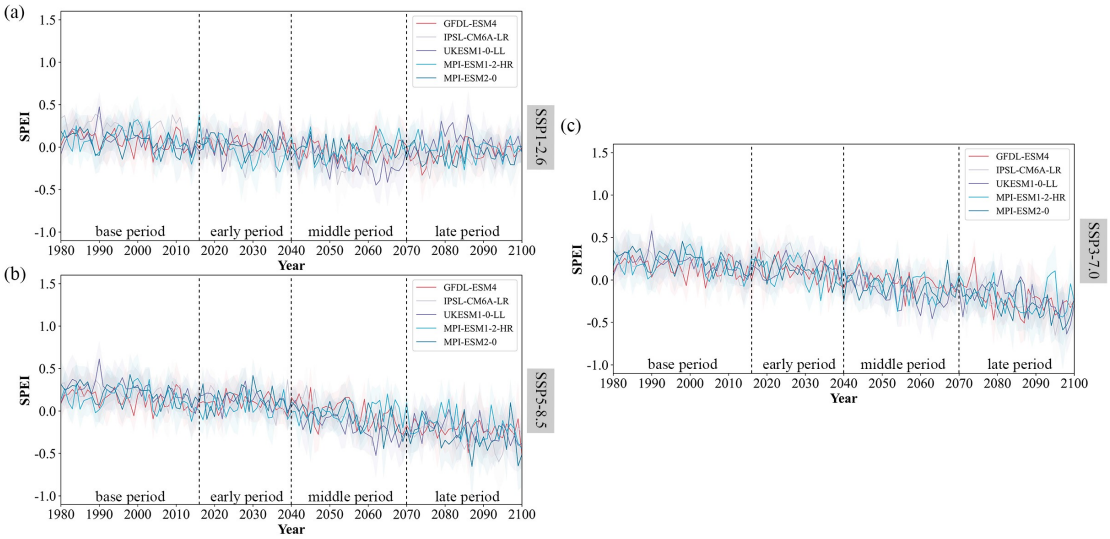

Supplementary Figure 3. Interannual variation of daily SPEI (PET calculated from PM-RC) under (a) SSP1-2.6, (c) SSP3-7.0 and (b) SSP5-8.5. Note: the solid line represents the annual mean of all global grids, while the shades represent the lower (25th percentile) and upper limits (75th percentile).

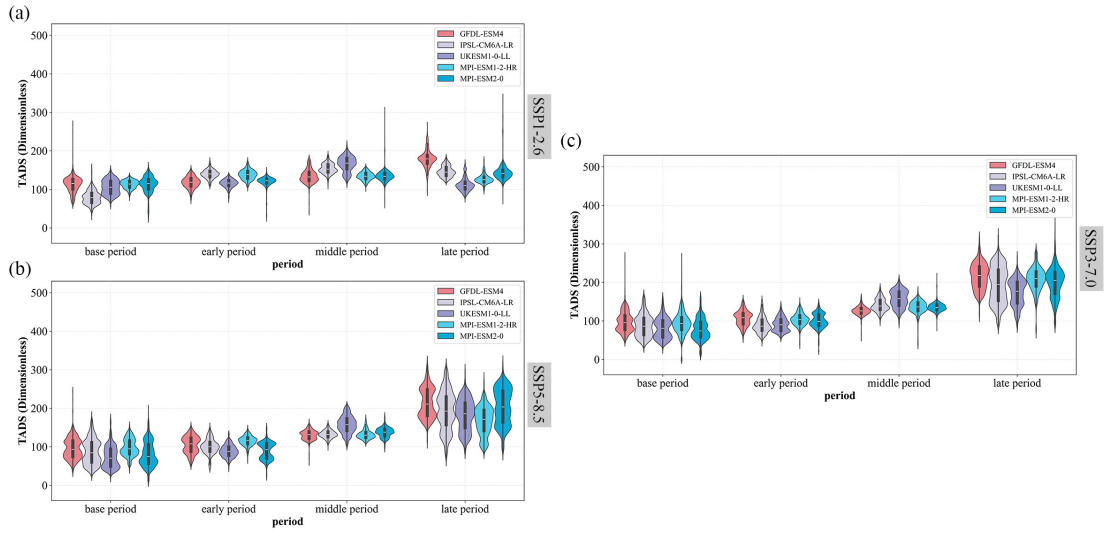

Supplementary Figure 4. Total annual drought severity (PET calculated from PM-RC) for the base period (1980–2014) and three future periods (2015–2040, 2041–2070, and 2071–2100) under (a) SSP1-2.6, (c) SSP3-7.0 and (b) SSP5-8.5.

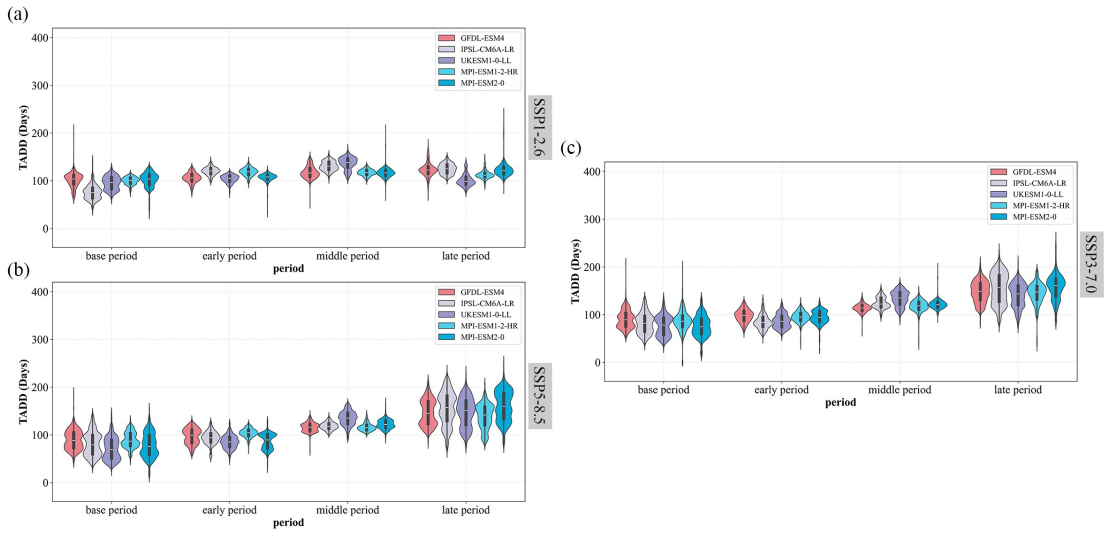

Supplementary Figure 5. Total annual drought duration (PET calculated from PM-RC) for the base period (1980–2014) and three future periods (2015–2040, 2041–2070, and 2071–2100) under (a) SSP1-2.6, (c) SSP3-7.0 and (b) SSP5-8.5.

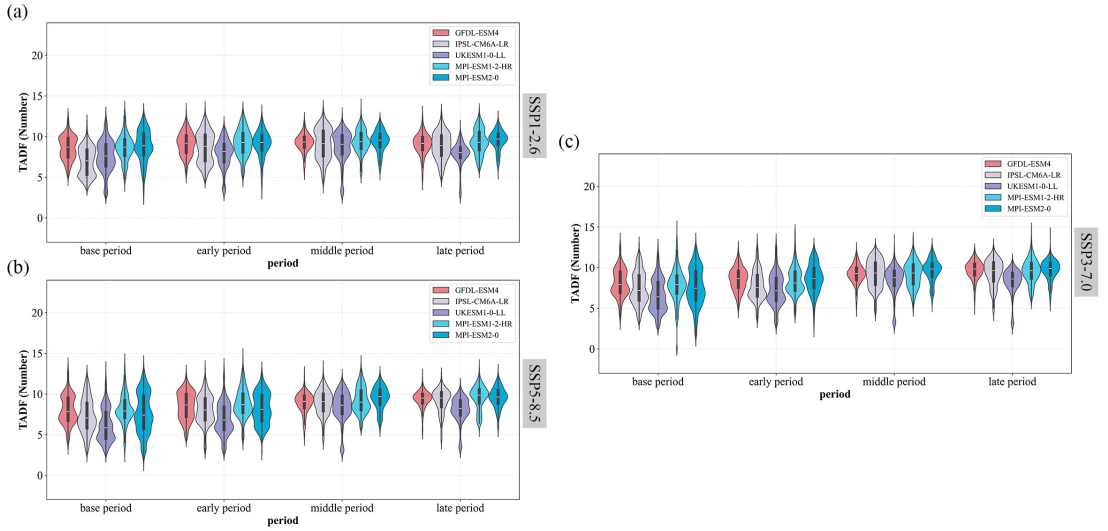

Supplementary Figure 6. Total annual drought frequency (PET calculated from PM-RC) for the base period (1980–2014) and three future periods (2015–2040, 2041–2070, and 2071–2100) under (a) SSP1-2.6, (c) SSP3-7.0 and (b) SSP5-8.5.

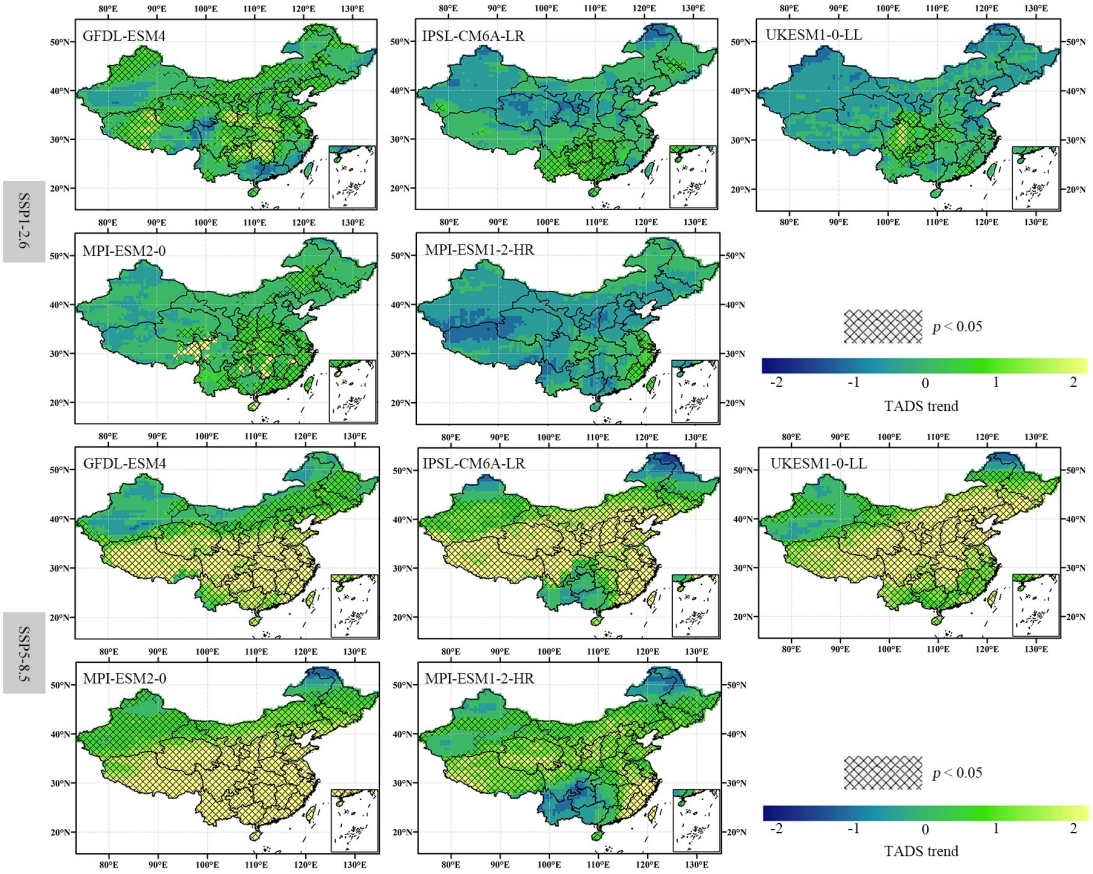

Supplementary Figure 7. Trends of TADS (PET calculated from PM-RC) from 2015-2100 by five GCMs under two SSP scenarios (spatial pattern).

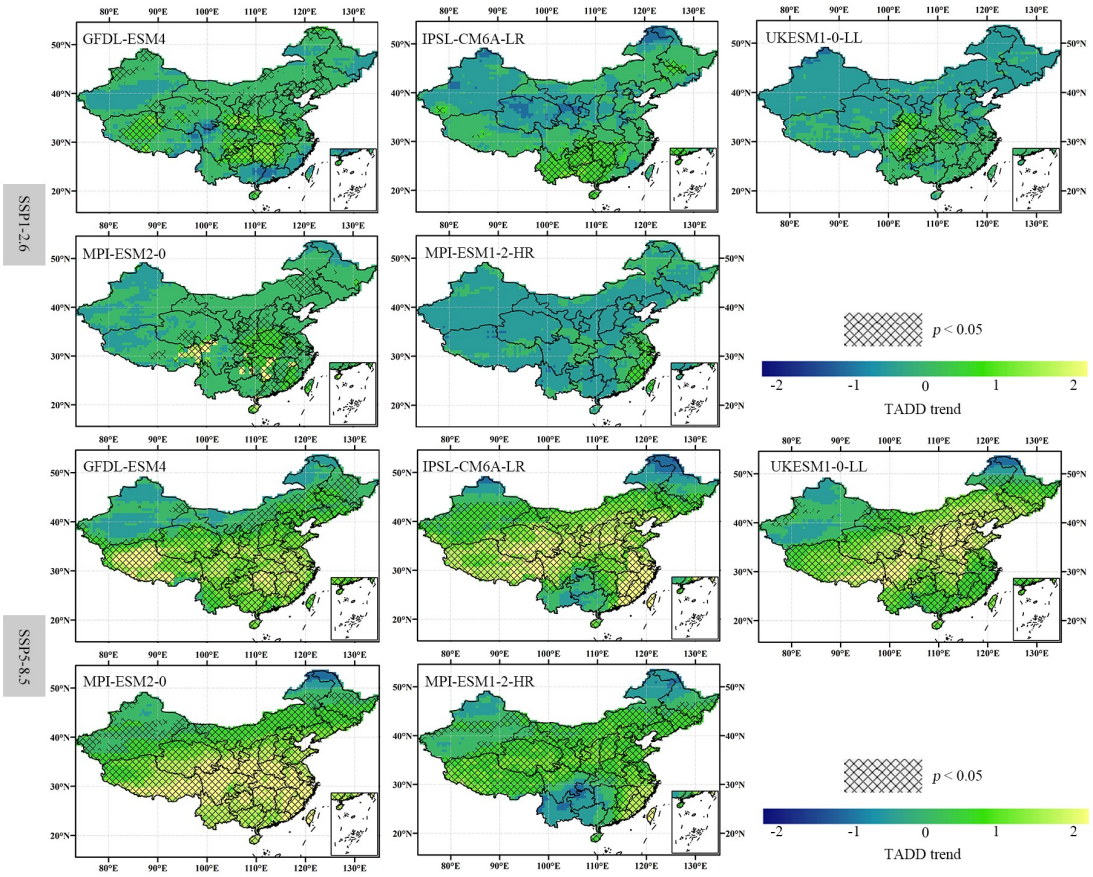

Supplementary Figure 8. Trends of TADD (PET calculated from PM-RC) from 2015-2100 by five GCMs under two SSP scenarios (spatial pattern).

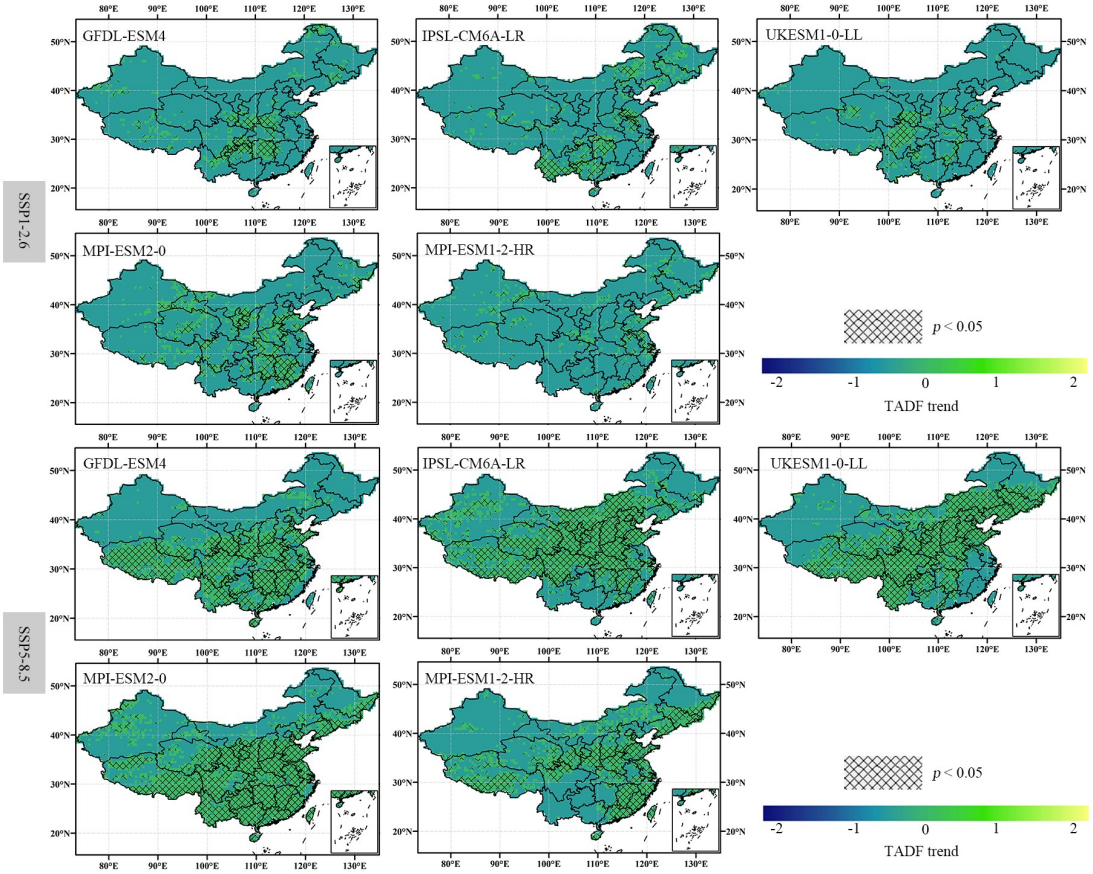

Supplementary Figure 9. Trends of TADF (PET calculated from PM-RC) from 2015-2100 by five GCMs under two SSP scenarios (spatial pattern).

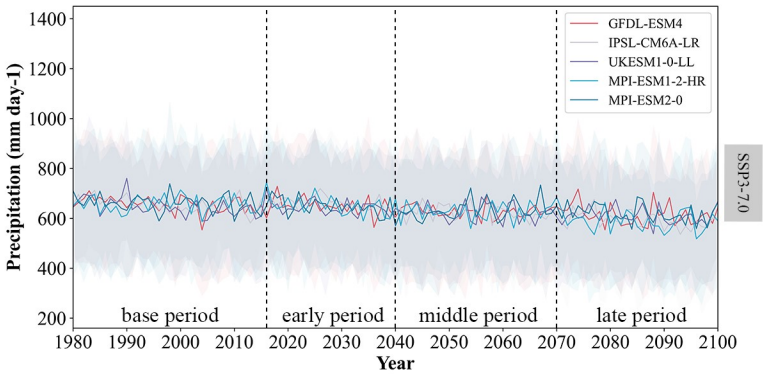

Supplementary Figure 10. Time series of precipitation under SSP3-7.0 by five GCMs. Note: the solid line represents the annual mean of all global grids, while the shades represent the lower (25th percentile) and upper limits (75th percentile).

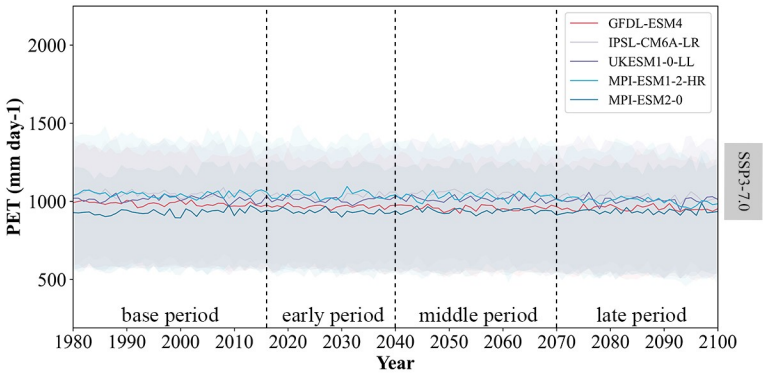

Supplementary Figure 11. Time series of PET calculated from PM-CO_2 under SSP3-7.0 by five GCMs. Note: the solid line represents the annual mean of all global grids, while the shades represent the lower (25th percentile) and upper limits (75th percentile).

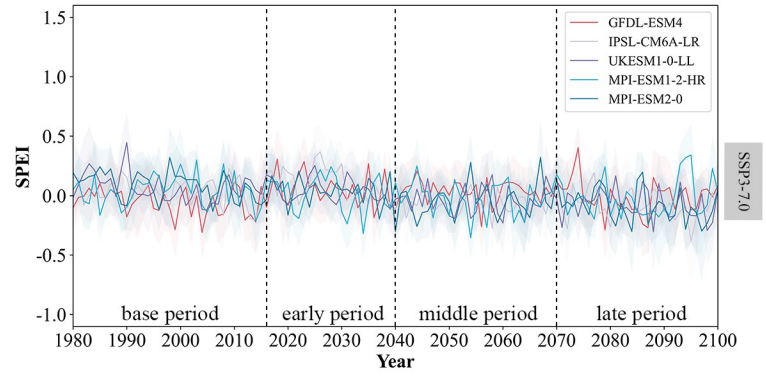

Supplementary Figure 12. Interannual variation of daily SPEI (PET calculated from PM-CO_2) under SSP3-7.0. Note: the solid line represents the annual mean of all global grids, while the shades represent the lower (25th percentile) and upper limits (75th percentile).

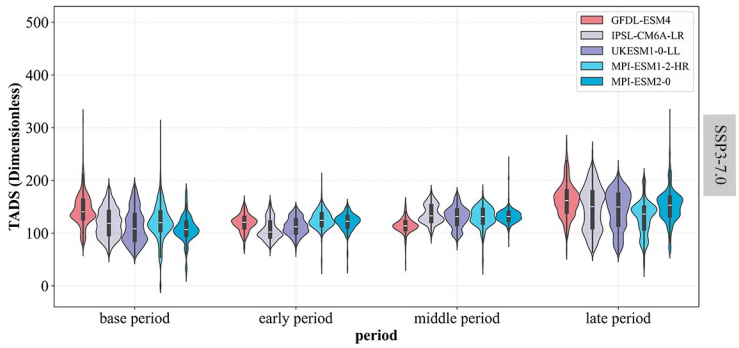

Supplementary Figure 13. Total annual drought severity (PET calculated from PM-CO_2) for the base period (1980 – 2014) and three future periods (2015 – 2040, 2041 – 2070, and 2071 – 2100) under SSP3-7.0.

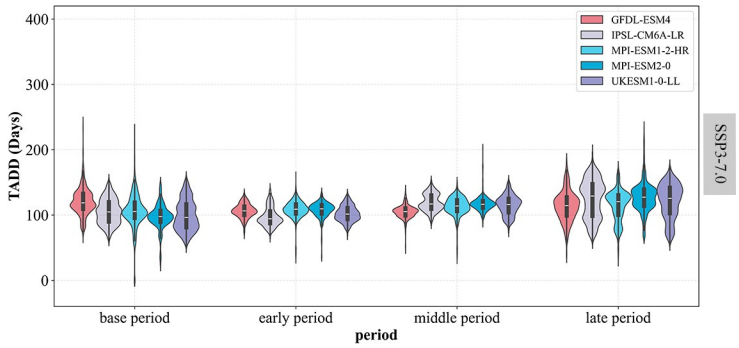

Supplementary Figure 14. Total annual drought duration (PET calculated from PM-CO_2) for the base period (1980 – 2014) and three future periods (2015 – 2040, 2041 – 2070, and 2071 – 2100) under SSP3-7.0.

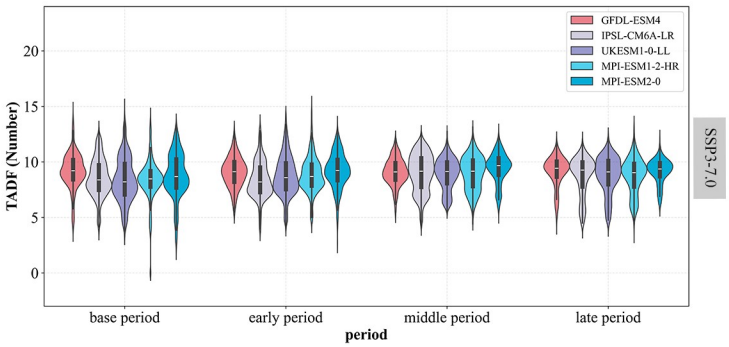

Supplementary Figure 15. Total annual drought frequency (PET calculated from PM-CO_2) for the base period (1980 – 2014) and three future periods (2015 – 2040, 2041 – 2070, and 2071 – 2100) under SSP3-7.0.

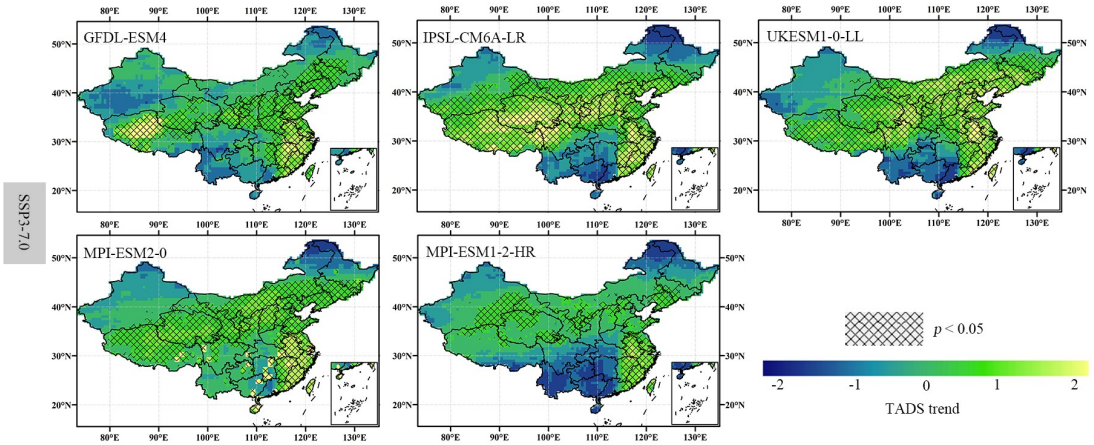

Supplementary Figure 16. Trends of TADS (PET calculated from PM-CO_2) from 2015-2100 by five GCMs under SSP3-7.0 (spatial pattern).

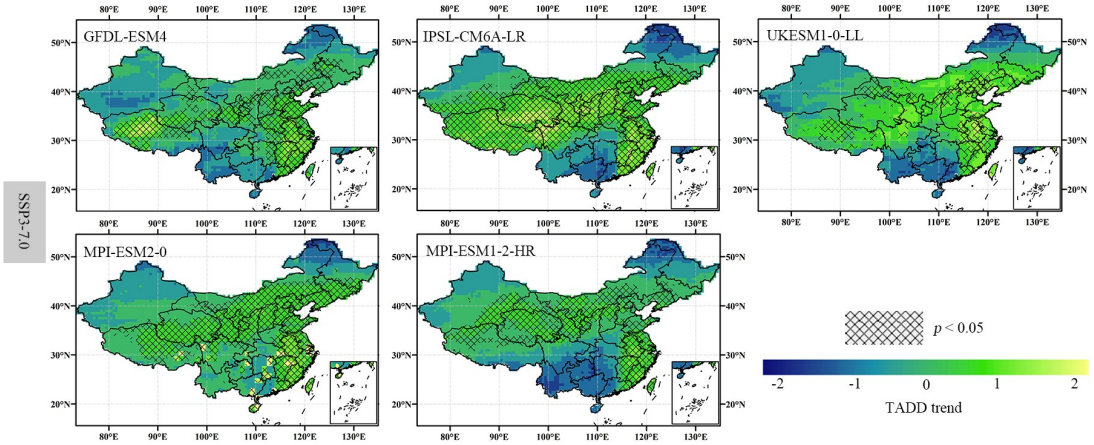

Supplementary Figure 17. Trends of TADD (PET calculated from PM-CO_2) from 2015-2100 by five GCMs under SSP3-7.0 (spatial pattern).

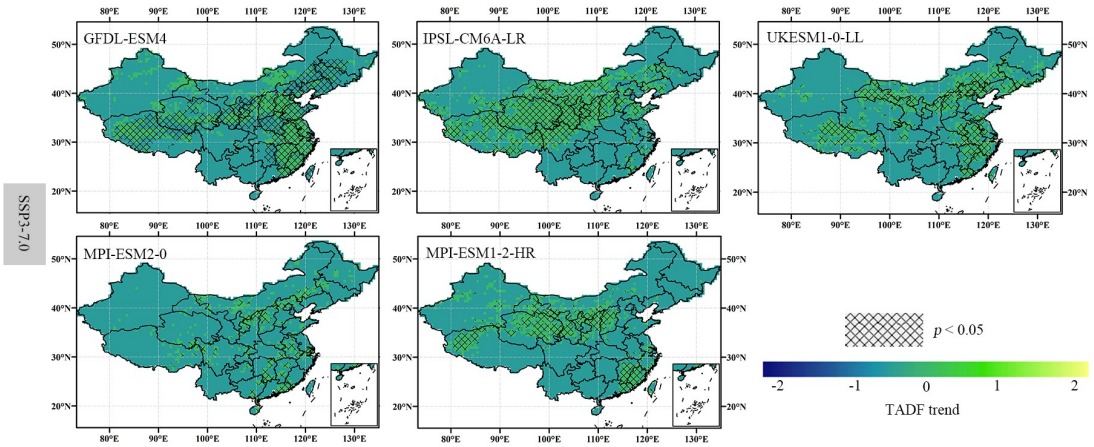

Supplementary Figure 18. Trends of TADF (PET calculated from PM-CO_2) from 2015-2100 by five GCMs under SSP3-7.0 (spatial pattern).

Supplementary References

1 Sai Krishna, S. V. S., Manavalan, P. & Rao, P. V. N. Estimation of Net Radiation using satellite based data inputs. *The International Archives of the Photogrammetry, Remote Sensing and Spatial Information Sciences* **XL-8**, 307-313, (2014).